Soft Computing (2023) 27:10921–10940
https://doi.org/10.1007/s00500-023-08253-2

APPLICATION OF SOFT COMPUTING

A driver authentication system integrated to stress-level determination for driving safety

Idil Isikli Esener[1]

Accepted: 13 April 2023 / Published online: 30 April 2023

Abstract
This paper analyzes the effects of electrocardiogram, electromyogram, respiration, hand and foot galvanic skin response signals on biometric identification using the features extracted through a similar process, which the author has previously introduced for drivers' distress recognition. This process consists of time-domain statistical feature extraction and a subspace-based feature selection. The utilization of subspace features is observed to increase the identification accuracy and decrease the execution time. Besides, the foot galvanic skin response signal is found to be more sensitive to identification among other signals, and increased stress level causes increased false negativity and hence decreased accuracy. These outcomes show that driver identification can be achieved by a process similar to the previously proposed for distress recognition, even using just one wearable technology without the need for any other equipment, and thus give the possibility to realize driver-customized infotainment and vehicle security applications using a single system.

Keywords Biometric identification · Feature extraction · Statistical features · Subspace decomposition · Classification

1 Introduction

The widespread use of biometric identification systems not only in security systems but also in daily routines such as public services, banking transactions, and patient follow-up increased the importance of studies on these systems. Although these studies can be analyzed based on what the person knows, what the person has, or who the person is, the "who the person is" policy is found to be more reliable for identification rather than the other two policies since the access security of the relevant systems can easily decrease in case of information and/or instrument. On the other side, quantitatively measurable biometric characteristics that exist in all people but with individual differences are utilized for the "who the person is" policy.

The biometric systems implemented on the "who the person is" policy conventionally use the physiological or behavioral characteristics, and alternatively cognitive characteristics, on the basis of what the person thinks. This paper focuses on the "who the person is" policy using physiological characteristics. Among these characteristics, fingerprint analysis (Cao and Jain 2019; Zeng et al. 2019; Chen et al. 2022) leads the face (Yang et al. 2007; Gowda et al. 2018; Zangeneh et al. 2020; Ferrari et al. 2021; Zhang et al. 2022), retina (Farzin et al. 2008; Rani and Rani 2019), iris (Ananth 2017; Park et al. 2018; Ahmadi and Akbarizadeh 2020), palm vein (Yang et al. 2007; Ali and Razuqi 2017), finger vein (Qin et al. 2017), hand geometry (Kanhangad et al. 2011; Ramalho et al. 2012), hand vein (Wang et al. 2015), ear shape (Prakash and Gupta 2014), and eye gesture (Lyamin and Cherepovskaya 2017) biometrics, for identification. These studies have spread to a wider area with the use of electrocardiogram (ECG) (Alemán-Soler et al. 2016; Alonso et al. 2016; Rezgui and Lachiri 2016; Lei et al. 2016; Wieclaw et al. 2017; Blasco and Peris-Lopez 2018; Labati et al. 2019; Abdeldayem and Bourlai 2020; Choi et al. 2020, 2021, 2022a; Kim et al. 2020a, b; Hwang et al. 2021; Srivastva et al. 2021, 2022; Zhou et al. 2021; Pereira et al. 2022), electroencephalogram (EEG) (Wang et al. 2020a; Zhang et al. 2020; Seha and Hatzinakos 2020; Wilaiprasitporn et al. 2019; Jin et al. 2021), Galvanic Skin Response (GSR) (Alonso et al. 2016; Blasco and Peris-Lopez 2018), electromyogram (EMG) (Alonso

✉ Idil Isikli Esener
idil.isikli@bilecik.edu.tr

[1] Department of Electrical Electronics Engineering, Bilecik Seyh Edebali University, 11210 Bilecik, Turkey

et al. 2016; Kim and Pan 2017; Lee et al. 2017; Shin et al. 2017; Shioji et al. 2017, 2018; Morikawa et al. 2018; Lu et al. 2019, 2020; Khan et al. 2020; Li et al. 2020; Jiang et al. 2020; Pradhan et al. 2021; Choi et al. 2022a; Pleva et al. 2022), and respiration (RESP) (Chauhan et al. 2017; Liu et al. 2020; Wang et al. 2022a, b) measurements. Studies using multiple signals for increased performance of identification in terms of both stability and accuracy are encountered in the literature (Alemán-Soler et al. 2016; Alonso et al. 2016; Blasco and Peris-Lopez 2018; Choi et al. 2022a).

The ECG signal is found to dominate the biometric identification studies in the recent literature (Abdeldayem and Bourlai 2020; Choi et al. 2020, 2021, 2022a, b; Kim et al. 2020a; Hwang et al. 2021; Srivastva et al. 2021; Zhou et al. 2021; Pereira et al. 2022; Srivastva et al. 2022) since it is evaluated to be more robust to impostors due to its physical contact requirement for measurement rather than the traditional biometric characteristics such as fingerprint, face, and iris (Nazmy et al. 2010; Dantcheva and Ross 2015; Kim et al. 2020a). Besides the advantages of an ECG signal, like being a unique characteristic inside the body of any individual and invulnerability to spoofing attempts, it has significant disadvantages of being easily affected by physiological and psychological conditions and correspondingly fluctuating nonlinearly (Choi et al. 2020, 2021; Hwang et al. 2021; Zhou et al. 2021). Studies in the related literature try to compensate for this shortcoming by using the ECG signals collected under various physiological/psychological conditions (Choi et al. 2020, 2021; Zhou et al. 2021; Hwang et al. 2021), normalizing the ECG signals having different heart rate patterns (Lin et al. 2014; Nobunaga et al. 2017; Choi et al. 2020, 2021; Hwang et al. 2021), or using the two-dimensional (2-D) representations (Kim et al. 2020b; Choi et al. 2022a, b) of ECG signals.

An intelligent transport system (ITS) in vehicles is an evolving subtopic of biometric systems consisting of driver-customized infotainment and vehicle security applications (Işıklı Esener 2021; Choi et al. 2021, 2022b). These applications include driver identification (Silva et al. 2012; Pinto et al. 2017; Santos et al. 2018; Choi et al. 2021, 2022a, b), stress recognition (Sihem et al. 2019), stress-level recognition (Munla et al. 2015; Işıklı Esener 2021), health condition recognition (Singh et al. 2016; He et al. 2019), mood/emotion recognition (He et al. 2019; Wang et al. 2020b), fatigue recognition (Shiwu et al. 2011; Wang et al. 2019), motion recognition (Kim and Choi 2019), voice recognition (Song et al. 2016), and cognitive distraction recognition (Miyaji et al. 2010a, b).

In the case of driving identification systems, the dominance of ECG signal utilization and focus on increasing the identification performance against the shortcomings of ECG signals by using their normalized (Choi et al. 2021) or 2-D transformed (Choi et al. 2022a, b) profiles are observed as in overall biometric systems. Besides, Choi et al. presented an increased accuracy when ECG and EMG signals of drivers are used together instead of single-handedly (Choi et al. 2022a).

In this study, identification performance improvement is intended using multiple signals by removing the negative effect of various stress states not only on heart rate but also on all signals. In accordance with this intent, a feature extraction scheme similar to the process, which the author has previously introduced for drivers' distress recognition (Işıklı Esener 2021), is examined for driver identification. This scheme is applied to the ECG, EMG, RESP, Hand GSR, and Foot GSR signals collected by Healey and Picard (2005) in the publicly available MIT-BIH PhysioNet Multi-parameter Database (Goldberger et al. 2000). The mentioned feature extraction process is composed of two phases (Işıklı Esener 2021). The first phase is designed for time-domain statistical feature extraction on the above signals, while the second phase is for feature selection, performing Discriminative Common Vector (DCV) approach on the extracted features in the first phase. The driver detection process in this paper is then defined as a ten-class classification problem using both feature sets obtained in each phase. The Fisher's Linear Discriminant Analysis (FLDA), Linear Discriminant Classifier (LDC), Logistic Linear Classifier (LLC), and Random Forest (RF) classifiers are performed via a fivefold cross-validation technique in the classification stage.

Utilization of time-domain statistical features satisfies a maximum of 98.30% accuracy for identification, while it is increased to 100% by using subspace features in 11.31% less execution time, using the RF classifier. The use of DCV that projects the data into a subspace that is the same within but different between classes, also enables the projection of statistical features into a subspace that is independent of the changeable stress levels, naturally. Besides, since dimension reduction is achieved by subspace decomposition, the system complexity increment caused by using multiple signals is also extenuated.

Besides analyzing all signals separate from each other, the Foot GSR signal is determined as being more sensitive to identification among other signals with an accuracy of almost 98% using both statistical and subspace features. To the best of the author's knowledge, the Foot GSR signal is introduced for biometric identification for the first time in this study, and comparable accuracy is achieved.

Finally, the stress levels of drivers are studied in terms of their effects on identification. This part of the study is concluded by an increased false negativity and hence decreased accuracy with the increment in stress level. The

analysis of the effects of stress level on identification indicates another novelty of this paper.

This paper is organized as follows: in the following section, a literature overview related to this study is introduced. In Sect. 3, the utilized database is described, and technical information on the applied methods is given, while the performed experimental studies, including feature extraction and classification processes, are explained in detail in Sect. 4. In Sect. 5, the accomplished results are discussed, and finally, in Sect. 6, the main conclusions are indicated.

2 Literature overview

Although various biometric system studies have been carried out based on the physiological signals utilized in this study, the use of ECG signals is found to be more intense in biometric authentication studies in the literature. The 2-D image transformations of ECG signals take part in recent related studies. Srivastva et al. experienced PlexNet learning for an ECG-based authentication system on the Check Your Biosignals Here initiative (CYBHi) and Physikalisch-Technische Bundesanstalt (PTB) datasets (Srivastva et al. 2021). A zero-phase 4th-order bandpass filter with cut-off frequencies of 0.5 and 30 Hz was utilized for noise removal, and heartbeats were segmented as 700 ms-length windows centered at R-peaks detected by Pan-Tompkins algorithm (Pan and Tompkins 1985). The sequential three z-score normalized heartbeat segments are concatenated to form 150 × 150-dimensional representations. These 2-D ECG images are directly fed to a Convolutional Neural Network (CNN) architecture, and an authentication accuracy of 99.66% was achieved for both CYBHi and PTB databases. Any information about time consumption for the proposed system is not given in the paper. Pereira et al. proposed scalogram-based template generation for authentication and verified their proposal on the CYBHi database (Pereira et al. 2022). The authors initially applied a bandpass filter of degree 4 with cut-off frequencies of 0.5 and 30 Hz on the ECG signals belonging to 63 subjects. Then, the heartbeats were segmented using Nerokit2 (Makowski et al. 2021), and each segment was subjected to min–max normalization. These normalized segments were transformed to a 2-D scalogram representation of size 56 × 56 performing Continuous Wavelet Transform (CWT) via Morse wavelet with $\gamma = 3$ and $P^2 = 60$. All the scalograms of any subject were concatenated to form the corresponding 1 × 188,160-dimensional template, resulting in a 63 × 188,160-dimensional training/testing set. Independent Component Analysis (ICA) was applied with 63 independent components on this set to reduce the computational cost of the template-matching algorithm. Finally, a Manhattan distance-based template-matching algorithm was performed for authentication, and an accuracy of 98.42% was achieved. The authors state that they did not perform any time consumption calculation, but both the scalogram generation and ICA implementation were time-consuming operations. In another study, Kim et al. examined a similar process on the MIT-BIH Normal Sinus Rhythm Database (NSRDB) (Kim et al. 2020b). Bandpass filtering, median filtering, and first-order regression analysis were implemented for noise removal, and heartbeat cycles were detected using the Pan-Tompkins algorithm (Pan and Tompkins 1985) in the study. The 2-D representation of an ECG signal was obtained by applying linear projection to the pre-processed 1-D signal, using its amplitude value. An ensemble of CNN architectures was then fed by these 2-D ECG images for authentication, and an accuracy of 98.9% was achieved. Abdeldayem and Bourlai used spectral correlation analysis for projecting a 1-D pre-processed ECG signal into its 2-D representation of size 128 × 128 (Abdeldayem and Bourlai 2020). These images were the inputs of the CNN network for authentication. The authors verified their proposal on NSRDB, MIT-BIH Arrhythmia Database, PTB, and many other ECG databases. Authentication accuracies of 98.7%, 96.5%, and 94.7% were satisfied on these databases, respectively. Besides, studies performing statistical (Srivastva et al. 2022; Alemán-Soler et al. 2016; Alonso et al. 2016; Hwang et al. 2021; Zhou et al. 2021), morphological (Choi et al. 2020, 2021), frequency-domain (Blasco and Peris-Lopez 2018), and CNN-based (Lei et al. 2016) feature extraction exist in the literature as well as the studies did not employ feature extraction (Wieclaw et al. 2017; Alonso et al. 2016).

The utilization of EMG signals, as well as ECG signals, in biometric identification studies, has become widespread in recent years. Lee et al. mooted that people could be recognized by their walking habits, and in line with this idea, they examined the EMG signals measured from the low-limb muscles of 12 subjects (Lee et al. 2017). The root mean square, mean absolute value, dominant frequency, integrated EMG signals, and onset time of EMG signals were the features extracted from the limb EMG signals in this study. They utilized the Linear Discriminant Analysis (LDA) classifier with these features and achieved an overall accuracy of 65.7%. Kim and Pan experienced an ensemble of time-domain and frequency-domain features extracted from EMG signals for simultaneous motion and personal recognition (Kim and Pan 2017). They verified their proposal on two databases: a self-acquired EMG dataset and a publicly available UCI dataset. Their self-acquired dataset consists of 4 subjects' EMG signals measured from the extensor carpi radial and the flexor carpi

ulnaris at two channels, under making a fist, rotating the wrist, and raising the hand movements. Waveform length was used for time-domain feature extraction, while a non-uniform filter bank was applied for frequency-domain feature extraction. Besides, principal component analysis (PCA) and LDA were performed for dimension reduction. Euclidean distance, Support Vector Machines (SVM), and k-nearest neighbor classifiers were used for classification in the study, and the highest personal recognition accuracy is stated as 85% on the self-acquired dataset using the Euclidean distance classifier, while it is 88.66% on the UCI dataset. It is also indicated that simultaneous motion recognition succeeded with accuracies of 95% and 84.66% on the self-acquired and UCI datasets, respectively, by following the same process. Shin et al. collected forearm EMG signals under making a fist, opening hand, and wrist shaking up/down tasks (Shin et al. 2017). Low-pass, high-pass, and notch filters with cut-off frequencies of 200 Hz, 0.5 Hz, and 60 Hz, respectively, were applied to the signals for noise removal. Statistical feature extraction was realized on the filtered signals, and 5-dimensional feature vectors were constructed, including variance, mean, zero-crossing, length, and median frequency of the signals. It is stated that authentication was realized with an accuracy of 81.6% when these features were used in an artificial neural network. Shioji et al. reported that they could simultaneously achieve hand motion recognition and personal authentication with an accuracy of $\sim$ 94.5% for each, using the eight-channel EMG signals measured from eight subjects' wrists while they were performing Japanese Janken gestures: "paper," "scissors," and "rock" (Shioji et al. 2018). Feature extraction and authentication were realized using a CNN model in the study. The authors also state that they could authenticate individuals with an accuracy of 96.7% using the EMG signals collected during performing only "paper" motion (Shioji et al. 2017). Lu et al. utilized a 2-D representation of EMG signals for personal identification (Lu et al. 2019). The 1-D EMG signals of length 300 were collected from 21 subjects' right forearms through eight channels using the Myo Armband device. The CWT via Mexican Hat wavelet was applied to these signals to get their 2-D representations of size 32×300. Then, a CNN architecture was employed for both time–frequency domain feature extraction and classification. The authors state an accuracy of 99.203% following this process. In their posterior study, the authors pre-processed the data they collected in Lu et al. (2019) by applying a four-level discrete wavelet transform via the Daubechies wavelet and obtained five subbands of each channel (Lu et al. 2020). Statistical feature extraction (variance, standard deviation, and root mean square value) was realized on each subband, resulting in 120-dimensional feature vectors (8 channel $\times$ 5 subbands $\times$ 3 features) for each subject. An accuracy of 99.206% is indicated when ExtraTreesClassifier was used for identification. Li et al. proposed using surface EMG-based biometric information to improve the security of pattern unlock (Li et al. 2020). The authors collected 20 trials of EMG signals from 10 subjects on the flexor digitorum superficialis muscle of the forearm. The signals were high-pass and notch filtered for artifact and power-line noise removal, and filtered signals were partitioned into 2-s duration segments. Time-domain statistical feature extraction was realized from each segment resulting in 55-dimensional feature vectors of each subject by concatenating the mean absolute value, variance, high-order temporal moment, mean square root, root mean square, log detector, waveform length, difference absolute standard deviation value, and a number of zero-crossings of each segment. The classification was realized by SVM and local outlier factor classifiers and concluded with accuracies F1-scores of 0.97653 and 0.98202, respectively. Khan et al. proposed biometric authentication using the EMG signals of speech (Khan et al. 2020). A dataset of 10 subjects was acquired by measuring the EMG signals from the neck. These signals were segmented into 10-s duration segments which were then subjected to empirical mode decomposition for artifact and noise removal. Both time and frequency-domain feature extraction were performed on the pre-processed segments. The feature vectors consisting of Shannon energy, mean frequency, power bandwidth, peak to root mean square, 4th, 5th, 9th, 10th, and 12th coefficients of Chroma, zero-crossing rate, complexity factor, Higuchi fractal dimension, sparseness, irregularity factor, simple square integral, spectral roll-off, spectral flatness, spectral crest, and spectral spread were introduced to the quadratic SVM classifier, and an accuracy of 95.3% was achieved in the study. In another study, Morikawa et al. examined EMG signals measured from lips for personal authentication but concluded with a very low accuracy value is stated in the study (Morikawa et al. 2018). Pleva et al. practiced EMG signals for computer system user identification (Pleva et al. 2022). The authors collected forearm EMG signals via the Myo Armband device from 64 channels while users had been typing the word "password". They extracted 13 Mel-frequency cepstral coefficients from each of the 500 ms-duration EMG frames of each user. It is stated that an identification accuracy of 96.45% was achieved by feeding a 1-D CNN network with these coefficients. In a similar study, Jiang et al. collected high-density surface EMG signals from 22 subjects' right dorsal hands while entering finger muscle isometric contraction password (FMICP) (Jiang et al. 2020). Noise removal and power line interference attenuation were achieved by an 8th-order 10–900 Hz Butterworth bandpass filter and a 50 Hz Notch filter, respectively. Finally, the filtered signals were

segmented into eight 3-s duration tasks. Macroscopic- and microscopic-level features were extracted from these tasks. Macroscopic-level features were stated as sample entropy, spectral entropy, frequency median, waveform length, and root mean square computed in the time–frequency domain from each channel, resulting in 320-dimensional feature vectors per subject. Microscopic-level features were defined as the concatenation of average firing rates of the motor unit spike trains of each task and across all tasks obtained by ICA, resulting in 9-dimensional feature vectors per subject. Utilizing these features, equal error rates (EERs) of 0.0128 and 0.1496 were succeeded when wrong and correct FMCIPs were entered, respectively.

Identification studies using just RESP signals are rarely seen in literature. Chauhan et al. proposed a new behavioral biometric signature based on audio features derived from an individual's commonplace breathing gestures (Chauhan et al. 2017). This authentication mechanism (BreathPrint) uses the audio signatures associated with the three individual gestures: sniff, normal, and deep breathing, which are sufficiently different across individuals. Using these three breathing gestures, they developed the processing pipeline that identifies users via the microphone sensor on smartphones and wearable devices. Using off-the-shelf hardware, they experimentally evaluated the BreathPrint prototype with 10 users, observed over seven days. They showed that users could be authenticated reliably with an accuracy of over 94% for all three breathing gestures. Wang et al. presented a Multi-user Authentication system (M-Auth), for capturing the user's unique breathing pattern that employs a single COTS mmWave radar which exploits the phenomenon that radio frequency signals are affected by chest displacements due to breathing (Wang et al. 2022b). They proposed a signal energy comparison method to eliminate irrelevant body movements for preserving fine-grained respiration traits. Then, they developed a feature selection pipeline to elicit the most informative features and trained a machine learning-based classifier to identify each user. To eliminate repetitive and less informative features, they used the Recursive Feature Elimination (RFE) method to analyze the extracted features. Specifically, they used a linear kernel SVM classifier as the estimator for RFE. The classifier was trained by starting with all 70 features via fivefold cross-validation. Extensive experiments involving 37 participants (17 females and 20 males) whose ages range from 19 to 35 demonstrated that M-Auth is effective in verifying legitimate users and thwarting spoofing attacks, with an authentication accuracy of over 96% and an attack detection rate of over 95%. Liu et al. proposed a continuous user verification system, which re-uses the widely deployed WiFi infrastructure to capture the unique physiological characteristics rooted in the user's respiratory motions (Liu et al. 2020). They extracted the respiration-related signals from the channel state information of WiFi. Then they derived the user-specific respiratory features based on the waveform morphology analysis and fuzzy wavelet transformation of the respiration signals. Additionally, a deep learning-based user verification scheme was developed to identify legitimate users accurately and detect the existence of spoofing attacks. Experiments involving 20 participants (14 males and 6 females, aging from 21 to 32) demonstrate that the proposed system can verify users with high accuracy (over 91%) and is resilient to spoofing attempts.

Studies using only the GSR signal in the literature have generally been applied to stress/emotion/cognitive load detection (Kim et al. 2020c; Ayata et al. 2017; Setyohadi et al. 2018; Acevedo et al. 2021; Nourbakhsh et al. 2017; Tiwari and Agarwal 2021; Goshvarpour and Goshvarpour 2020), and distraction identification (Dehzangi et al. 2018).

The related literature also includes studies that support using multiple signals to increase identification accuracy. Alonso et al. used ECG, EMG, Hand GSR, airflow, temperature, and pulse oximetry signals for biometric authentication (Alonso et al. 2016). The authors realized this study using both the raw signals they collected from 25 subjects and the features extracted from these signals. They constructed a 12×1-dimensional feature vector consists of mean and skewness of oxygen saturation, mean and kurtosis of pulsioximetry, entropy and standard deviation of EMG, kurtosis of pulse, a standard deviation of airflow, a standard deviation of temperature, mean, standard deviation, and kurtosis of ECG signals. After all, PCA is applied to the feature vectors for dimension reduction. A True Positive Rate (TPR) of 40% was achieved when the linear SVM classifier was trained by the raw signals while using the 12×1-dimensional feature vectors increased this rate to 64%. Besides, if dimension-reduced features were utilized, TPRs of 84% and 92% succeeded with 10×1- and 9×1-dimensional feature vectors, respectively.

Blasco and Peris-Lopez examined the coexistence of photoplethysmography (PPG), ECG, Hand GSR, and accelerometer features for authentication (Blasco and Peris-Lopez 2018). These signals were self-acquired from 25 subjects and pre-processed by applying DC removal and bandpass filtering between 0.67 and 45 Hz for noise removal in the study. A feature vector of size 292×1 for each subject was constructed by concatenating the 32 Fourier Transform and 64 Walsh-Hadamard Transform lower coefficients of PPG, ECG, and accelerometer signals with mean, standard deviation, maximum, and minimum values of the Hand GSR signal. A Gaussian Mixture Model (GMM) was used for classification, and 0.99 area under the curve and 0.02 EER was reported in the study.

Although it is mostly preferred, in biometric systems, heart rate fluctuations observed in ECG signals due to physiological and/or psychological conditions adversely affect the identification performance. Therefore, it is thought that systems that ignore this mentioned negative effect or that are verified on ECG signals collected under a single state would not be reliable to run in real-life conditions. Hence, recent studies focus on eliminating this effect for increased identification accuracy. Zhou et al. proposed a feature extraction scheme for an ECG-based authentication system that addresses the shortcomings of conventional systems realized under the same psychological conditions (Zhou et al. 2021). Hence, they measured ECG signals from 23 subjects under three stress levels. They performed median filtering, a 4th-order zero-phase 30 Hz Butterworth high-pass filter, and a bandpass filter between 5 and 15 Hz for baseline drift, noise, and artifact removal, respectively. The Pan-Tompkins algorithm (Pan and Tompkins 1985) was performed for R-peak detection, and 25-dimensional statistical Heart Rate Variability (HRV) features were extracted from the detected RR intervals. The HRV features were processed via GMM in order to reduce the effect of stress on these features. The authors defined this process as manual feature extraction. Besides, they realized automatic feature extraction using a 1-D CNN architecture. Authentication was realized using the ensemble of manual and automatic features via the SVM classifier and concluded with 97% accuracy. Choi et al. proposed a fusion normalization of ECG signals in order to match the post-exercise fiducials with the pre-exercise ones, thus improving the post-exercise authentication accuracy (Choi et al. 2020, 2021). The authors collected ECG signals from 100 subjects under rest-exercise-rest conditions. Morphological feature extraction was realized on the pre-processed post-exercise ECG signals, and authentication was satisfied with 98% accuracy via long short-term memory (LSTM) classifier. Hwang et al. proposed a nonlinear normalization to attenuate the effect of changes in heart rate to improve ECG-based authentication performance using ECG signals (Hwang et al. 2021). The authors verified their proposal on a self-acquired database of ECG signals measured from 15 subjects while they had been resting, listening to calm music, listening to exciting music, watching a relaxed video, watching a scary video, and exercising. They applied a 60 Hz Notch filter, a 3rd-order 0.5 Hz Butterworth high-pass filter, and wavelet decomposition for power line interference, baseline wandering, and artifact suppression, respectively. Then, they segmented the cardiac cycles as described by Martínez et al. (2004). As the final step of pre-processing, they applied a nonlinear normalization, based on the cardiac cycle, before the heart rate changes. Authentication was realized via the Gaussian SVM classifier using 29-dimensional fiducial features. The authors reported 99.05% accuracy when the rest-state-measured ECG signals were used, while an accuracy of 88.14% was achieved when all-state ECG signals were used. They succeeded with 93.55%, 90.87%, and 76.15% accuracies when signals measured while listening to calm music and watching a scary video, listening to exciting music and watching a relaxed video, and exercising were used, respectively. In line with these results, the authors claimed their proposal to be convenient to use for ECG-based authentication systems in various physical conditions.

The driver identification systems using the ECG signals also face the case in point. Choi et al. proposed an adaptive driver-specific threshold filtering-based normalization to reduce normalization-caused morphological feature distortion and motion artifacts due to the driving environment for an increased identification performance (Choi et al. 2021). The authors verified their proposal on a self-acquired dataset of ECG signals belonging to 100 subjects collected on the steering wheel, seat belt, and gear rod. Bandpass and moving-average filters were applied to the signals for noise removal, and zero calibration was performed for baseline wander suppression. The zero-calibrated signals were then segmented into cycles by fiducial point segmentation using the R-peaks detected by the Pan-Tompkins algorithm (Pan and Tompkins 1985), and adaptive filter-based normalization of each cycle was realized. The LSTM classifier was examined using these cycles, and a 95.4% accuracy of identification was achieved. In another study of the authors, they used the 2-D spectrograms of each cycle segmented in (Choi et al. 2021) in a CNN network and achieved an identification accuracy of 97.1% (Choi et al. 2022b). Choi et al. proposed a driver identification system and verified their system using the ECG and EMG signals of 6 subjects belonging to the MIT-BIH PhysioNet Multi-parameter Database (Choi et al. 2022a). They utilized the 2-D image representations of these signals obtained by constant Q transform as the CNN inputs. The authors stated identification accuracies of 84.4% and 98.1% when only EMG and ECG signals were used, respectively, while an increased accuracy of 98.9% succeeded when both signals were used. The achieved accuracy indicates that using multiple signals in addition to the compensation of HRV concludes with the best identification performance.

At this point in the literature overview, two important shortcomings attract the attention of identification studies using bio-signals: (1) real-life conditions cause heart rate fluctuations in ECG signals which deteriorate the identification accuracy, as may also be valid for other bio-signals, (2) utilizing multiple signals provides more accurate and stable systems, but also increase the system complexity. Addressing these shortcomings in this study, a subspace-

based feature extraction scheme for driver identification is proposed using five bio-signals of drivers. Subspace decomposition is realized via the DCV approach on an ensemble of celebrated statistical features extracted on the ECG, EMG, RESP, Hand GSR, and Foot GSR signals. Thus, the projection of statistical features into a subspace independent of the changeable stress levels is satisfied. Moreover, since dimension reduction is achieved by subspace decomposition, increased system complexity is also extenuated even though multiple signals are used. Additionally, the stress levels of drivers are studied in terms of their effects on identification in this study. Effects of various activities on identification are previously studied in the literature (Hwang et al. 2021), but to the author's knowledge, this study is the first analysis of the effects of stress levels on identification.

3 Materials and methods

3.1 Database

The effect of stress on biometry is analyzed using the MIT-BIH PhysioNet Multi-parameter Database (Goldberger et al. 2000). This database was prepared by Healey and Picard (2005), measuring the bio-signals of 17 healthy volunteer drivers via wearable sensors placed, as shown in Fig. 1, during three city- and two highway-driving between two resting states from MIT's East Garage to River Street Bridge. The measured ECG and EMG signals were sampled at 496 Hz and 15.5 Hz, respectively, while the sampling frequency is indicated as 31 Hz for Hand GSR, Foot GSR, and RESP signals (Healey and Picard 2005).

It is stated in the database that drivers have low stress (LS) levels at rest, while they have moderate stress (MS) and high stress (HS) levels during highway- and city-driving, respectively. In addition to the bio-signals, the database also consists of a marker signal for each driver, which indicates the crossings between consecutive drivings. All these signals for a sample driver are shown in Fig. 2 as an example of the database.

3.2 Stress-level determination

In this study, a feature extraction process similar to the one which the author previously introduced for distress recognition of automobile drivers (Işıklı Esener 2021) is proposed for a robust driver identification system. This scheme, for stress-level determination, consists of time-domain statistical feature extraction on (1) Heart Rate (HR) signals derived from the ECGs, (2) EMG, (3) RESP, (4) Hand GSR, and (5) Foot GSR signals followed by subspace decomposition of these features using the DCV approach (Işıklı Esener 2021). Then, each driver is classified as having LS, MS, or HS via linear SVM classifier using the decomposed features. The time-domain statistical features consist of the maximum, mean, median, standard deviation, the difference between the maximum and minimum, and the difference between the median and mean of HR, Hand GSR, Foot GSR, and EMG signals, root mean square, root mean quad, and zero-crossing rate of EMG signals concatenated by the RESP features. The RESP features are the minimum, maximum, average, and standard deviation of the respiration rate, minimum, maximum, and average breathing durations, difference between the maximum and minimum breathing durations, minimum, maximum, and average breathing amplitudes, difference between the maximum and minimum breathing amplitudes, range, standard deviation, skewness, and kurtosis computed on the RESP signals.

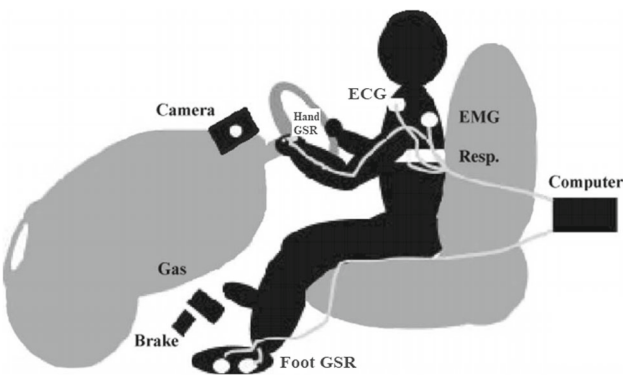

Fig. 1 Bio-signal collection (Healey and Picard 2005)

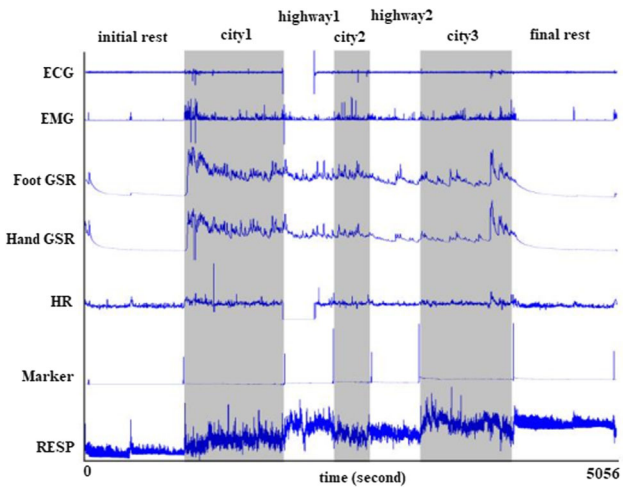

Fig. 2 Measured bio-signals for a sample driver (Keshan et al. 2015)

3.3 Feature extraction

The signals utilized in this paper for biometric identification are changeable due to the physiological and biological effects of stress. Therefore, to characterize the related changes, time-domain statistical feature extraction on ECG, EMG, GSR, and respiration RESP signals, similar to the one introduced in Işıklı Esener (2021), is realized.

3.3.1 HR features

It is already known that stress can cause irregular heartbeat and/or arrhythmia by affecting the heart (Keshan et al. 2015). The frequency and the regularity of the heartbeats are monitored via the ECG. Hence, HR features are derived from the ECG signals.

The functioning of a heart is determined by analyzing the P, Q, R, S, and T waveforms of an ECG, shown in Fig. 3. The number of R-peaks of an ECG signal indicates the number of heartbeats, while the duration between any two consecutive R-peaks is the time between sequential heartbeats. The terms "dur." and "amp." in Fig. 3 refer to duration and amplitude, respectively. The durations and amplitudes of QRS complex, Q-wave, and S-wave show clinical significance in terms of any existence of abnormality. This inference is also observed as the stress level changes rather than the existence of any abnormality, as can be seen in the HR signal in Fig. 2. In this paper, it is analyzed whether this inference can be used for personal identification. Hence, the same statistical features, characterizing the amplitude changes in ECG signals, in Işıklı Esener (2021) are extracted.

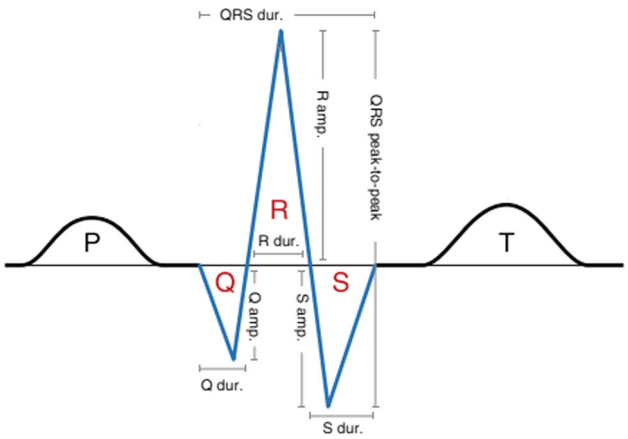

Fig. 3 Important waveforms on a sample ECG signal (Norland et al. 2019)

3.3.2 GSR features

Skin conductance measured from the palms and the sole of the feet can easily change due to any emotional and mental stimuli since they have a high density of sweat glands. The amplitude changes of Foot GSR and Hand GSR signals in different stress levels can be seen in Fig. 2. Moreover, skin conductance may be correlated with personal characteristics such as stability and lability. In line with this idea, rather than the personality type, the feasibility of identifying a person using skin conductivity information is examined in this paper. For this examination, similar statistical features characterizing the amplitude changes in Hand GSR and Foot GSR signals extracted for distress recognition in Işıklı Esener (2021) are utilized.

3.3.3 EMG features

Stress, distress, and any other emotional or mental stimuli are known to increase muscular tension, as can be validated by analyzing the sample EMG signal shown in Fig. 2. This tension variation between different stress levels is analyzed in terms of person identification in this paper, by using a subset of the statistical features extracted in Işıklı Esener (2021). The statistical features extracted from the HR, Hand GSR, Foot GSR, and EMG signals are given in Table 1. Most of the time-domain statistical features extracted from the RESP signals for distress recognition in Işıklı Esener (2021) are used for personal identification in this paper. These features are given in Table 2.

The mathematical representations of the above-mentioned features are given in Table 3. The term $\vec{X}$ in the table refers to the N-dimensional signal from which features are to be extracted.

3.4 Subspace decomposition

3.4.1 Discriminative common vector approach

The discriminative common vector (DCV) of any given class is a unique vector capable of representing all the vectors within that class (Cevikalp et al. 2005). The DCV approach consists of two stages. In the first stage, the common vector of the cth class, $\vec{X}^c_{\text{com}}$, is achieved by projecting any of N vectors, $\vec{X}^c_i$, in that class onto the null space of within-class scatter matrix S_w of all S classes.

$$S_w = \sum_{c=1}^{S} \sum_{i=1}^{N} \left(\vec{X}^c_i - \vec{\mu}^c\right) \cdot \left(\vec{X}^c_i - \vec{\mu}^c\right)^T \tag{1}$$

$$\vec{\mu}^c = \frac{1}{N} \cdot \sum_{i=1}^{N} \vec{X}^c_i \tag{2}$$

Table 1 Time-domain statistical features extracted from the HR, Hand GSR, Foot GSR, and EMG signals

HR, Hand GSR, Foot GSR, and EMG features	
Minimum	Maximum
Mean	Median
Standard deviation	Variance
Difference between maximum and minimum values (maximum–minimum)	
Difference between median and mean values (median–mean)	

Table 2 Time-domain statistical features extracted from the RESP signals

RESP features	
Number of breathings	Number of breathings
Minimum breathing duration	Minimum breathing duration
Maximum breathing duration	Maximum breathing duration
Average breathing duration	Average breathing duration
Maximum–minimum of the breathing duration	Maximum–minimum of the breathing duration
Minimum breathing amplitude	Minimum breathing amplitude

Table 3 The mathematical representations of the time-domain statistical features

Feature	Mathematical representation
Minimum	$\min = \text{minimum}\left\{ \overrightarrow{X}(i) \middle\| i = 1, 2, \cdots N \right\}$
Maximum	$\max = \text{maximum}\left\{ \overrightarrow{X}(i) \middle\| i = 1, 2, \cdots N \right\}$
Mean	$\mu = \frac{1}{N} \cdot \sum_{i=1}^{N} \overrightarrow{X}(i)$
Standard deviation	$\sigma = \sqrt{\frac{1}{N-1} \cdot \sum_{i=1}^{N} \left(\overrightarrow{X}(i) - \mu \right)^2}$
Variance	$\sigma^2 = \frac{1}{N-1} \cdot \sum_{i=1}^{N} \left(\overrightarrow{X}(i) - \mu \right)^2$
Median	$\text{med} = \overrightarrow{X}\left(\frac{N+1}{2}\right)$
Maximum–minimum	$\max - \min$
Median–mean	$\lvert \text{med} - \mu \rvert$
Skewness	$\frac{1}{\sigma^3} \cdot \sum_{i=1}^{N} \left(\overrightarrow{X}(i) - \mu \right)^3$
Kurtosis	$\frac{1}{\sigma^4} \cdot \sum_{i=1}^{N} \left(\overrightarrow{X}(i) - \mu \right)^4$
Zero-crossing rate (ZCR)	$\text{ZCR} = \frac{1}{2N} \cdot \sum_{i=2}^{N} \left(\text{sgn}\left(\overrightarrow{X}(i) \right) - \text{sgn}\left(\overrightarrow{X}(i-1) \right) \right)$ $\text{sgn}\left(\overrightarrow{X}(i) \right) = \begin{cases} 1, \overrightarrow{X}(i) \geq 0 \\ -1, \overrightarrow{X}(i) < 0 \end{cases}$
Number of breathings	Number of zero-crossings
Breathing interval	interval from one respiration (one zero-crossing) to another
Breathing duration (in ms)	$60000 \cdot \frac{\text{length(Breathing Interval)}}{\text{length(1 minute)}}$
Breathing amplitude	$\lvert \text{Breathing Interval} \rvert$

In the second stage, the discriminative common vector of the c^{th} class, $\overrightarrow{\Omega}^c$, is obtained by projecting the common vector $\overrightarrow{X}^c_{\text{com}}$ of that class onto the difference space of the between-class scatter matrix of the common vectors, S_{com}, which is computed as given in Eq. (3).

$$S_{\text{com}} = \sum_{c=1}^{S} \left(\overrightarrow{X}^c_{\text{com}} - \overrightarrow{\mu}_{\text{com}} \right) \cdot \left(\overrightarrow{X}^c_{\text{com}} - \overrightarrow{\mu}_{\text{com}} \right)^T \tag{3}$$

$$\overrightarrow{\mu}_{\text{com}} = \frac{1}{S} \cdot \sum_{c=1}^{S} \overrightarrow{X}^c_{\text{com}} \tag{4}$$

3.5 Classification

3.5.1 Fisher's linear discriminant analysis

The main idea of the Fisher's linear discriminant analysis (FLDA) is to find a projection matrix ω, onto a subspace where training samples from different classes are accurately separated by satisfying the Fisher maximization criterion, $J(\vec{\omega})$, which means the between-class variance is maximized while the within-class variance is minimized (Fisher 1936).

$$J(\vec{\omega}) = \frac{\omega^T \cdot S_B \cdot \omega}{\omega^T \cdot S_W \cdot \omega} \tag{5}$$

The terms ω, S_B, and S_W in Eq. (5) refer to projection matrix, between-class scatter matrix, and within-class scatter matrix, respectively. For an S-class classification problem, any test vector is assigned to class c, so that the Euclidean distance, $\|\vec{\Omega}^c - \vec{\Omega}_{\text{test}}\|$, between the projected test vector, $\vec{\Omega}_{test}$, to the projected mean vector, $\vec{\Omega}^c$, of training samples in class c, is minimum. This decision criterion, K, for the FLDA is formulized as given in Eq. (6).

$$K = \underset{1 \le c \le S}{\operatorname{argmin}} \left\{ \|\vec{\Omega}^c - \vec{\Omega}_{\text{test}}\| \right\} \tag{6}$$

3.5.2 Linear discriminant classifier

The linear discriminant classifier (LDC) is a binary classifier that finds a linear discriminative hyperplane $g(\vec{x})$ of training samples $\vec{x}$ as given in Eq. (7) (Webb 2002). The terms $\vec{\omega}$ and ω_0 in this equation are the weight vector and the bias of the linear hyperplane, respectively.

$$g(\vec{x}) = \vec{\omega}^T \cdot \vec{x} + \omega_0 \tag{7}$$

In the testing stage of the LDC, any test sample $\vec{x}_{\text{test}}$ is projected onto this hyperplane, and then assigned to class w_i according to the sign of the $g(\vec{x}_{\text{test}})$.

$$g(\vec{x}_{\text{test}}) = \vec{\omega}^T \cdot \vec{x}_{\text{test}} + \omega_0 \tag{8}$$

$$\vec{x}_{\text{test}} \in \begin{cases} w_1, & g(\vec{x}_{\text{test}}) > 0 \\ w_2, & g(\vec{x}_{\text{test}}) < 0 \end{cases} \tag{9}$$

3.5.3 Logistic linear classifier

The logistic linear classifier (LLC) defines the linear hyperplane $g(\vec{x})$ in Eq. (7) as the logarithm of the rate of class-conditional probability density function $p(\vec{x}|w_i)$ of training samples $\vec{x}$ for each class w_i as given in Eq. (10), and any test sample $\vec{x}_{test}$ is classified to the class with the highest sample-conditional probability $p(w_i|\vec{x}_{\text{test}})$ (McLachlan 1992). The terms $\vec{\omega}$ and ω_0 in Eq. (10) refer to the weight vector and the bias of the linear hyperplane, respectively.

$$g(\vec{x}) = \vec{\omega}^T \cdot \vec{x} + \omega_0 = \log\left(\frac{p(w_1|\vec{x})}{p(w_2|\vec{x})}\right) \tag{10}$$

Assuming equal prior probabilities $p(w_i)$ and covariance matrices for each class, the sample-conditional probability density functions of $\vec{x}$ are computed as:

$$p(w_1|\vec{x}) = \frac{\exp\left(\vec{\omega}^T \cdot \vec{x} + \omega_0\right)}{1 + \exp\left(\vec{\omega}^T \cdot \vec{x} + \omega_0\right)}$$

$$p(w_2|\vec{x}) = \frac{1}{1 + \exp\left(\vec{\omega}^T \cdot \vec{x} + \omega_0\right)} \tag{11}$$

The decision criterion for the LLC can either be formulated as in Eq. (13) or Eq. (14).

$$g(\vec{x}_{\text{test}}) = \vec{\omega}^T \cdot \vec{x}_{\text{test}} + \omega_0 = \log \tag{12}$$

$$\vec{x}_{\text{test}} \in \begin{cases} w_1, & \dfrac{p(w_1|\vec{x}_{\text{test}})}{p(w_2|\vec{x}_{\text{test}})} > 1 \Rightarrow p(w_1|\vec{x}_{\text{test}}) > p(w_2|\vec{x}_{\text{test}}) \\ w_2, & \dfrac{p(w_1|\vec{x}_{\text{test}})}{p(w_2|\vec{x}_{\text{test}})} < 1 \Rightarrow p(w_2|\vec{x}_{\text{test}}) > p(w_1|\vec{x}_{\text{test}}) \end{cases} \tag{13}$$

$$\vec{x}_{\text{test}} \in \begin{cases} w_1, & g(\vec{x}_{\text{test}}) > 0 \\ w_2, & g(\vec{x}_{\text{test}}) < 0 \end{cases} \tag{14}$$

3.5.4 Random forest

A decision tree classifier creates a model for data clustering by defining simple classification rules (Safavian and Landgrebe 1991). Following these defined rules in the training stage, the classification of any test sample is realized in the test stage. Decision tree classifiers differ from each other by their strategy for rule definition. The random forest classifier aims to improve classification accuracy by constructing multiple decision trees with different strategies in the training stage and combining their outputs via a majority voting technique in the test stage (Breiman 2001).

4 Experimental study

In this paper, the previously proposed subspace-based feature extraction scheme performed on HR, EMG, RESP, Hand GSR, and Foot GSR signals for stress recognition of

drivers (Işıklı Esener 2021), is studied in terms of biometric identification using the MIT-BIH PhysioNet Multiparameter Database (Goldberger et al. 2000). Although this database consists of bio-signals of 17 drivers, measurements of 10 drivers, whose record names are given in Table 4, are utilized for the experiments since the rest 7 drivers have missing signals or unclear information about the signals. The block diagram of the proposed study is given in Fig. 4.

4.1 Pre-processing

Bio-signals suffer from baseline wander and muscle- and body movement-related noises. Hence, a noise reduction process is highly necessary for better feature extraction. Additionally, R-peak detection on ECG signals is needed to determine the heart rate and HRV features. Table 5 summarizes these pre-processing operations realized in this paper. Besides the operations given in this table, all the signals are partitioned into 1-min-duration windows without overlapping.

4.2 Feature vector construction

The feature extraction is realized on the 1-min-durated partitions of the pre-processed signals. The 14-min recordings of each distress level are used in this paper.

The feature vector construction scheme in which statistical time-domain feature extraction is performed as well as the features obtained in this way are called "statistical" in this paper, while the feature vector construction scheme carried out by applying DCV decomposition on the statistical features and subsequently obtained features are called "subspace".

The distress levels of the drivers are stated as LS, MS, and HS during rest states, highway-driving, and city-driving, respectively, in the dataset. Five types of feature vectors are obtained by the mentioned feature construction schemes. These are the statistical feature vectors extracted from the measurements recorded during rest states, highway, and city drives, concatenation of overall features, and subspace features obtained by DCV decomposition on the concatenation of overall statistical features. The constructed feature vectors are given in Table 6.

Table 4 List of drivers whose bio-signals are used in this paper (Işıklı Esener 2021)

Record names				
drive5	drive6	drive7	drive8	drive9
drive10	drive11	drive12	drive15	drive16

4.2.1 Statistical feature vector construction

The time-domain statistical features given in Tables 1 and 2 are extracted from the per-minute partitions of each measurement. Then, these feature vectors of each signal are concatenated, forming the resultant 44-dimensional statistical feature vector for each partition of each driver. This scheme is described in Table 7.

4.2.2 Subspace feature vector construction

The subspace feature vector of each driver is constructed as 9-dimensional vectors obtained by the DCV decomposition on his statistical feature vector.

4.3 Classification

The biometric identification of automobile drivers in this paper is a ten-class classification problem and is achieved via both statistical and subspace feature vector construction processes. The classification scheme consists of experiments performed using FLDA, LDC, LLC, and RF classifier via a fivefold cross-validation technique. It means that features extracted from 11-min records (80%) and the remaining 3-min records (20%) of each driver are used as training and test data, respectively, in each fold.

4.4 Performance evaluation

The performance of statistical and subspace feature extraction schemes for biometric identification are individually evaluated in this paper. Besides, the effect of stress level on biometric identifiability is also commentated by analyzing the outcomes achieved by using feature vectors extracted on each signal type and during each stress level separately. These outcomes are given in terms of sensitivity (SNS), specificity (SPC), Positive Predictive Value (PPV), Negative Predictive Value (NPV), False Positive Rate (FPR), False Negative Rate (FNR), False Discovery Rate (FDR), False Omission Rate (FOR), and accuracy (ACC) metrics. These metrics are computed on the total confusion matrices of each experiment by using the mathematical expressions given in Table 8. The total confusion matrix of an experiment is constituted as the sum of confusion matrices computed in each fold of this experiment.

5 Results and discussion

In this paper, biometric identification of automobile drivers is implemented, and outcomes of this implementation are interpreted in terms of the feature vector construction

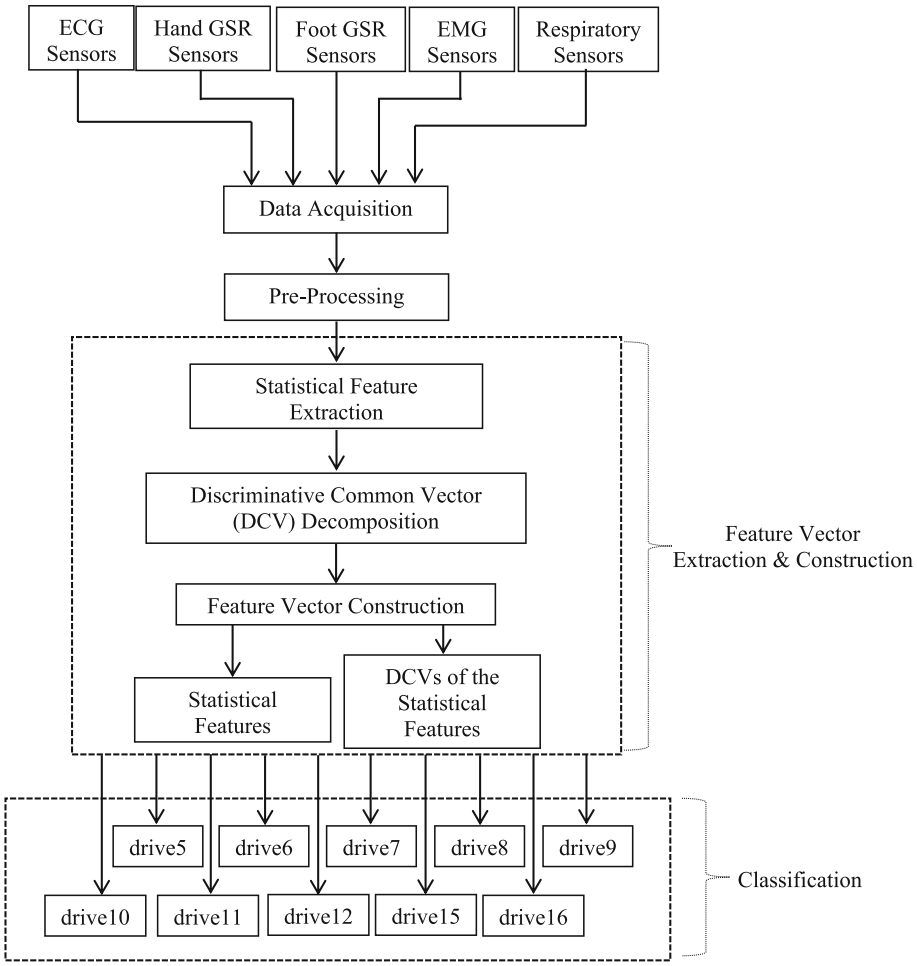

Fig. 4 Block diagram of the proposed study

Table 5 Pre-processing procedure

Signal	Operation	Parameters
ECG	Bandpass filter	Low cut-off frequency: 0.5 Hz
		High cut-off frequency: 4 Hz
ECG	R-peak detection and HR signal derivation	Inverted second derivative method (Zhang et al. 2012)
GSR	Butterworth bandpass filter	Low cut-off frequency: 0.1 Hz
		High cut-off frequency: 1 Hz
Respiration	Moving-average filter	Cut-off frequency: 1 Hz
	Low-pass filter	
EMG	Butterworth low-pass filter	Cut-off frequency: 500 Hz

process, effects of stress level on authentication, and how well the signals were a good biomarker for identification. Related experiments are carried out using the MATLAB® tool on a computer with I5-7200U at 2.5 GHz and 8 GB memory.

Initially, the 132-dimensional overall statistical features, given in Table 6, are used for identification via the FLDA, LDC, LLC, and RF classifiers. The average performance evaluation metrics achieved in this experiment, given in Fig. 5, point to the identification power of the statistical features by a maximum accuracy of 98.30% using the RF classifier.

Although almost 100% accuracy and specificity are achieved in this case, relatively low sensitivity is caused by the FNs. False negativity of any class is a measure of how often that class is misclassified into a different class.

Table 6 Feature vector construction processes

Construction scheme	Feature type	Dimension
Statistical	Rest state features	44×1
	Highway drive features	44×1
	City drive features	44×1
	Overall features	132×1
	$= \begin{bmatrix} \text{Rest state features} \\ \text{Highway drive features} \\ \text{City drive features} \end{bmatrix}$	
Subspace	Overall features	9×1

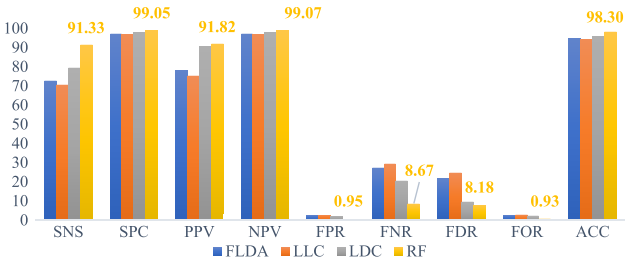

Fig. 5 The performance evaluation metrics achieved using the statistical feature vectors

The total confusion matrix computed in this experiment is given in Table 9, where rows and columns indicate the actual and predicted classes, respectively. This table clearly

Table 7 Statistical feature vector construction for driver identification

Statistical feature vector construction		
HR/Hand GSR Foot GSR/EMG features	RESP features	Statistical feature vector
8×1 for each signal	12×1	44×1
Minimum	Number of breathings	
Maximum	Minimum breathing duration	$\begin{bmatrix} \text{HR Features} \\ \text{Hand GSR Features} \\ \text{Foot GSR Features} \\ \text{EMG Features} \\ \text{RESP Features} \end{bmatrix}$
Mean	Maximum breathing duration	
Median	Average breathing duration	
Standard deviation	Maximum–minimum of the breathing duration	
Variance	Minimum breathing amplitude	
Maximum–minimum	Maximum breathing amplitude	
Median–mean	Average breathing amplitude	
	Maximum–minimum of the breathing amplitude	
	Standard deviation	
	Skewness	
	Kurtosis	

Table 8 Mathematical representations of the performance evaluation metrics

Performance evaluation metrics	Mathematical representations
TP: True Positive *TN*: True Negative *FP*: False Positive *FN*: False Negative	
Sensitivity (SNS)	$\%\text{SNS} = \frac{\text{TP}}{\text{TP+FN}} \cdot 100$
Specificity (SPC)	$\%\text{SPC} = \frac{\text{TN}}{\text{TN+FP}} \cdot 100$
Positive predictive value (PPV)	$\%\text{PPV} = \frac{\text{TP}}{\text{TP+FP}} \cdot 100$
Negative predictive value (NPV)	$\%\text{NPV} = \frac{\text{TN}}{\text{TN+FN}} \cdot 100$
False positive rate (FPR)	$\%\text{FPR} = \frac{\text{FP}}{\text{FP+TN}} \cdot 100$
False negative rate (FNR)	$\%\text{FNR} = \frac{\text{FN}}{\text{TP+FN}} \cdot 100$
False discovery rate (FDR)	$\%\text{FDR} = \frac{\text{FP}}{\text{TP+FP}} \cdot 100$
False omission rate (FOR)	$\%\text{FOR} = \frac{\text{FN}}{\text{TN+FN}} \cdot 100$
Accuracy (ACC)	$\%\text{ACC} = \frac{\text{TP+TN}}{\text{TP+TN+FP+FN}} \cdot 100$

Table 9 Total confusion matrix computed using the statistical feature vectors

Drive	5	6	7	8	9	10	11	12	15	16
5	15	0	0	0	0	0	0	0	0	0
6	0	15	0	0	0	0	0	0	0	0
7	0	2	13	0	0	0	0	0	0	0
8	0	0	0	13	0	0	2	0	0	0
9	0	0	0	1	14	0	0	0	0	0
10	0	0	0	0	0	15	0	0	0	0
11	0	0	0	4	0	0	9	0	2	0
12	0	0	0	0	0	0	0	15	0	0
15	0	1	0	0	0	0	0	0	14	0
16	0	0	0	0	1	0	0	0	0	14

shows that the sensitivity will substantially increase if the number of FNs could be decreased. This inference is verified when subspace features are utilized in the second phase of the study.

The graphics in Fig. 6 explain the improvement of the performance evaluation metrics when subspace features are used regardless of the classifier. Analyzing the results achieved via the RF classifier, it is explicitly seen that the number of FNs is reduced to zero resulting in 0% FNR and FOR, while an SNS and an NPV of 100% are satisfied. Similarly, the decrement of FPs to zero provides an increment in SPC and PPV to 100%, along with the decrement in FPR and FDR to 0%. Consequently, biometric identification is realized 100% accurately using the subspace features. The same results are also achieved when the LLC classifier is used.

Analysis of the time costs of the realized experiments shows that the execution time for subspace feature vector construction is approximately 7.74% longer than for the statistical scheme. Nevertheless, a decrement of 14.20% and 59.41% in classification time is determined when the RF and LLC classifiers are used, respectively. Therefore, the use of the subspace features is found to shorten the overall process by 11.31% and 33.46% when RF and LLC classifiers are utilized, respectively. The time consumption comparison of the realized experiments is given in Table 10.

The driver identification studies in the literature can be researched under two categories using: (1) on-board sensor data and (2) bio-signals. The studies using on-board sensor data perform identification by analyzing the behavior of drivers (Jafarnejad et al. 2017; Miyajima et al. 2007; Wu and Ye 2009; Rahim et al. 2020; Kwak et al. 2020; Mekki et al. 2019; Marchegiani and Posner 2018; Nishiwaki et al. 2007; Fung et al. 2017; Burton et al. 2016; Zhao et al.

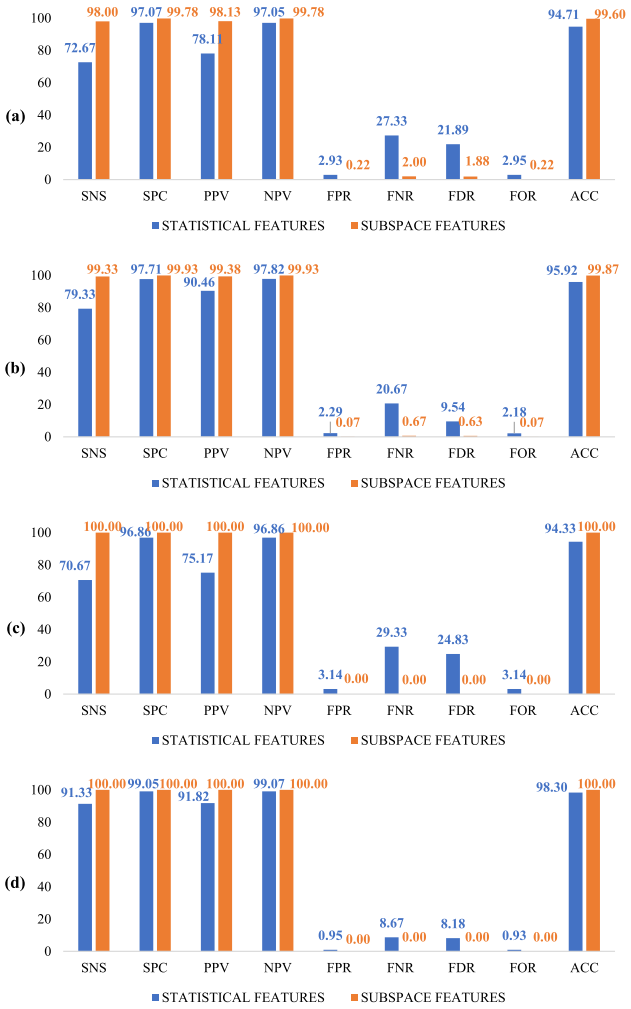

Fig. 6 Comparison of performance evaluation metrics achieved using the statistical versus subspace feature vectors via the **a** FLDA **b** LDC **c** LLC **d** RF classifiers

2022). The proposed process in this study is found to be more successful with 100% accuracy than studies mentioned above using on-board sensor data with a maximum of 96% accuracy (Rahim et al. 2020).

In the case of bio-signal utilization, the results achieved for driver identification using statistical and subspace features are compared with the related literature in Table 11. These studies, except (Choi et al. 2021), use only the ECG signals for identification. Silva et al. (2012) and Santos et al. (2018) did not consider heart rate fluctuations under various conditions, which is a questionable case in the literature for its applicability in real-life conditions (Choi et al. 2020, 2021; Hwang et al. 2021). From this perspective, the studies introduced by Choi et al. (2021, 2022b) are more relevant to this paper. These studies achieved accuracies of 95.4% and 97.1%, which are lower than the accuracy succeeded by the proposed process.

Table 10 The time consumption comparison of the realized experiments

	Execution time (s)			
	Statistical feature vectors		Subspace feature vectors	
Feature vector construction	5.1609		5.5602	
Classifier	RF	LLC	RF	LLC
Classification	34.0243	8.1935	29.1913	3.3259
Overall	39.1852	13.3544	34.7515	8.8861

Table 11 Comparison of the proposed system with the driving identification systems using bio-signals in the literature

References	Database	Bio-signal	Number of subjects	Method	Accuracy (%)
Silva et al. (2012)	Self-acquired	ECG	32	Euclidean distance classifier	70
Santos et al. (2018)	MIT-BIH PhysioNet Multi-Parameter Database	ECG	5	Fiducial feature extraction	95.8
				RF classifier	
Choi et al. (2021)	Self-acquired	ECG	100	Adaptive filter-based normalization	95.4
				LSTM classifier	
Choi et al. (2022a)	MIT-BIH PhysioNet Multi-Parameter Database	ECG	6	2-D CQT conversion	98.1
		EMG		CNN	84.4
		Multiple signals: ECG and EMG			98.9
Choi et al. (2022b)	Self-acquired	ECG	100	2-D spectrogram transformation	97.1
				CNN	
This paper	MIT-BIH PhysioNet Multi-Parameter Database	Multiple signals: ECG, EMG, Hand GSR, Foot GSR, and RESP	10	Time-domain statistical feature extraction	98.30
				RF classifier	
				Subspace-based feature extraction	100.00
				RF classifier (proposed)	
		ECG		Time-domain statistical feature extraction	93.71
		EMG			95.10
		Hand GSR		RF classifier	92.16
		Foot GSR			98.55
		RESP			95.98

Besides these, Choi et al. (2022a) presented a higher accuracy for driver identification than achieved using a single bio-signal when they used multiple signals in their proposed system to eliminate heart rate fluctuations in ECG signals. Although highly accurate systems are proposed, Choi et al. used the LSTM and CNN structures in the classification stage (Choi et al. 2021, 2022a, b), which theoretically have more complexity than the RF classifier utilized in this study. Besides the theoretical complexity of the pre-processing and classification methods used by Choi et al. the dimensions of the data they used as the inputs of CNN and LSTM architectures (50×50 and 65×23) are relatively higher than the RF input size, 9×1, used in the proposed process. These reveal the difference and superiority of this study to the literature not only in terms of accuracy but also complexity and computational cost per subject.

The effect of stress level on identification is analyzed by using the 44-dimensional statistical feature vectors in Table 7, extracted from the bio-signals measured during different stress levels separately in the classification process using the RF classifier. It is seen that, from the succeeded performance evaluation metrics given in Fig. 7, bio-signals measured when the subject is under low stress are more successful in biometric identification. The sensitivity, rather than the accuracy, of the system is found to

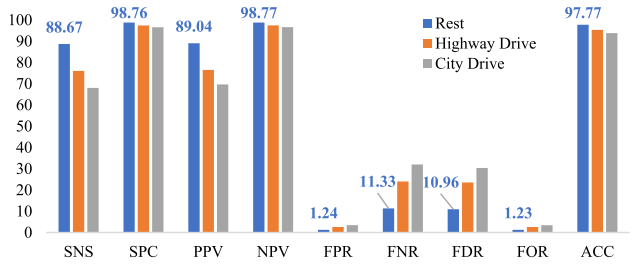

Fig. 7 The performance evaluation metrics achieved via the RF classifier, using the statistical feature vectors of each stress level

decrease considerably as the stress level increases. The reason for this decrement is examined through the increments in FPR and FNR, and it is concluded with higher false negativity provoked by the higher stress levels.

Finally, the identification ability of each bio-signal is analyzed by using the corresponding statistical features given in Table 7 during each stress level. Figure 8 shows the identification accuracies achieved in this analysis using the RF classifier. The "ALL SIGNALS" features in the figure refer to the 44-dimensional statistical features in Table 7, while the "OVERALL" feature of any signal is the 132-dimensional statistical feature constructed as given in Table 6. It is clear from the figure that the Foot GSR signal is a better biomarker for identification than other signals and even the concatenation of them.

6 Conclusions

Biometric identification using physical biometrics has become widespread, especially in security applications, because of the inseparability of the identifier from a person and the impossibility of creating a fake identifier. A similar process for feature extraction to the one which the author has previously introduced for drivers' distress recognition (Işıklı Esener 2021) is proposed for biometric identification

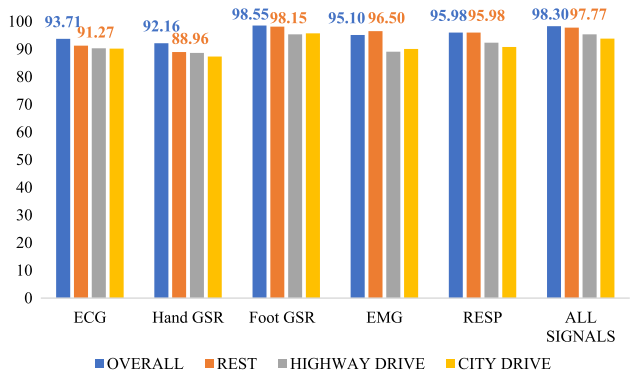

Fig. 8 Identification accuracies achieved via the RF classifier, using the statistical feature vectors extracted from each type of signal measured during each stress level

in this paper. The ECG, EMG, RESP, Hand GSR, and Foot GSR signals in MIT-BIH PhysioNet Multi-parameter Database are used to verify the proposed process. This process consists of time-domain statistical feature extraction and a subspace-based feature selection using the DCV approach. The use of the DCV approach both satisfies the projection into a subspace independent of the measurement environment and dimension reduction, which reduces the system complexity. The driver identification system presented in this paper is implemented by a ten-class classification problem. A maximum accuracy of 98.30% is achieved by utilizing the 132-dimensional time-domain statistical features, while it is increased to 100% by using the 9-dimensional subspace features. In addition to this increment in accuracy, an 11.31% reduction in execution time is satisfied. Comparing these results with the related literature explicitly indicates that the proposed process successfully meets the shortcomings of the identification studies using bio-signals.

Besides, the stress levels of drivers are studied in terms of their effects on identification, and it is concluded that increased stress level causes increased false negativity and hence decreased accuracy. This outcome reveals the possibility of driver identification being achieved simultaneously by the same process previously proposed for distress recognition. Thus, it will be possible to realize driver-customized infotainment and vehicle security applications using a single system. The stress-related studies in the literature are conducted on how stress can be used as a biomarker for the diagnosis of any disease (Alagendran et al. 2022), and which biomarkers can determine the level of stress (Liew et al. 2016; Betti et al. 2018; Işıklı Esener 2019, 2021; Iqbal et al. 2021; Nath and Thapliyal 2021; Azgomi et al. 2021; Azgomi and Faghih 2022; Momeni et al. 2022). Hence, the analysis of the effects of stress levels on identification indicates one of the novelties of this paper.

Finally, analyzing all features separate from each other, the Foot GSR signal is determined as being more sensitive to identification among other signals with an accuracy of almost 98% using both feature sets. This outcome shows that the proposed scheme is capable of carrying out person verification using only one wearable technology without the need for any other equipment. Furthermore, although skin conductance is studied in the literature for stress-level detection (Işıklı Esener 2019, 2021; Iqbal et al. 2021; Momeni et al. 2022), stress regulation (Azgomi et al. 2021; Azgomi and Faghih 2022), cognitive load monitoring (Gjoreski et al. 2021), analyzing psychophysiological reactions (Spelt et al. 2022; Fanti et al. 2022; Wiltshire et al. 2022; Han et al. 2022; Chong et al. 2022; Pineau et al. 2022; Wang et al. 2022c), predicting antidepressant response (Pineau et al. 2022), and emotion recognition

(Cosme et al. 2022; Centifanti et al. 2022; Baldini et al. 2022), it is not common to use the Foot GSR signal for biometric identification. This indicates another novelty of this paper.

Funding The authors have not disclosed any funding.

Data availability The dataset analyzed during the current study is available in the PhysioNet repository, https://physionet.org/content/drivedb/1.0.0/.

Declarations

Conflict of interest The author declares that she has no conflict of interest. This article does not contain any studies with human participants or animals performed by any of the authors.

References

Abdeldayem SS, Bourlai T (2020) A Novel approach for ECG-based human identification using spectral correlation and deep learning. IEEE Trans Biom Behav Identity Sci 2(1):1–14

Acevedo CMD, Gómez JKC, Rojas CAA (2021) Academic stress detection on university students during COVID-19 outbreak by using an electronic nose and the galvanic skin response. Biomed Signal Process 68:102756

Ahmadi N, Akbarizadeh G (2020) Iris tissue recognition based on GLDM feature extraction and hybrid MLPNN-ICA classifier. Neural Comput Appl 32:2267–2281

Alagendran S, Velayutha Prabhu S, Pushpa N, Ponraj M, Rajasekaran M, Fernandez-Saavedra G, Archunan G (2022) Chromogranin A in human saliva as putative biomarker of alzheimer's type dementia. Int J Adv Res Sci Commun Technol 2(2):124–130

Alemán-Soler NM, Travieso CM, Guerra-Segura E, Alonso JB, Dutta MK, Singh A (2016) Biometric approach based on physiological human signals. In: 3rd ınternational conference on signal processing and ıntegrated networks (SPIN). IEEE, pp 681–686

Ali YH, Razuqi ZN (2017) Palm vein recognition based on centerline. Iraqi J Sci 58(2):726–734

Alonso ADD, Travieso CM, Alonso JB, Dutta MK, Singh A (2016) Biometric personal identification system using biomedical sensors. In: 2nd ınternational conference on communication control and ıntelligent systems (CCIS). IEEE, pp 104–109

Ananth C (2017) Iris recognition using active contours. Int J Adv Res Innov Discov Eng Appl 2(1):27–32

Ayata D, Yaslan Y, Kamaşak M (2017) Emotion recognition via galvanic skin response: Comparison of machine learning algorithms and feature extraction methods. IU- J Electr Electron Eng 17(1):3147–3156

Azgomi HF, Cajigas I, Faghih RT (2021) Closed-loop cognitive stress regulation using fuzzy control in wearable-machine ınterface architectures. IEEE Access 9:106202–106219

Azgomi HF, Faghih RT (2022) Enhancement of closed-loop cognitive stress regulation using supervised control architectures. IEEE Open J Eng Med Biol 3:7–17

Baldini A, Frumento S, Menicucci D, Gemignani A, Scilingo EP, Greco A (2022) Subjective fear in virtual reality: a linear mixed-effects analysis of skin conductance. TechRxiv. Preprint. https://doi.org/10.36227/techrxiv.19387052.v1

Betti S, Lova RM, Rovini E, Acerbi G, Santarelli L, Cabiati M, Ry SD, Cavallo F (2018) Evaluation of an ıntegrated system of wearable physiological sensors for stress monitoring in working environments by using biological markers. IEEE Trans Biomed Eng 65(8):1748–1758

Blasco J, Peris-Lopez P (2018) On the feasibility of low-cost wearable sensors for multi-modal biometric verification. Sensors 18(9):2782

Breiman L (2001) Random forests. Mach Learn 45:5–32

Burton A, Parikh T, Mascarenhas S, Zhang J, Voris J, Artan NS, Li W (2016) Driver identification and authentication with active behavior modeling. In: 2016 12th international conference on network and service management (CNSM). IEEE, pp 388–393

Cao K, Jain AK (2019) Automated latent fingerprint recognition. IEEE Trans Pattern Anal Mach Intell 41(4):788–800

Centifanti LCM, Gillespie SM, Thomson ND (2022) Skin conductance responses to a discrete threat in virtual reality: associations with psychopathy and anxiety. J Psychopathol Behav Assess 44:39–50

Cevikalp H, Neamtu M, Wilkes M, Barkana A (2005) Discriminative common vectors for face recognition. IEEE Trans Pattern Anal Mach Intell 27(1):4–13. https://doi.org/10.1109/TPAMI.2005.9

Chauhan J, Hu Y, Seneviratne S, Misra A, Seneviratne A, Lee Y (2017) BreathPrint: breathing acoustics-based user authentication. In: Proceedings of the 15th annual ınternational conference on mobile systems, applications, and services, pp 278–291. https://doi.org/10.1145/3081333.3081355

Chen S, Guo Z, Li X, Yang D (2022) Query2Set: single-to-multiple partial fingerprint recognition based on attention mechanism. IEEE Trans Inf Forensics Secur 17:1243–1253

Choi GH, Ko H, Pedrycz W, Singh AK, Pan SB (2020) Recognition system using fusion normalization based on morphological features of post-exercise ECG for intelligent biometrics. Sensors 20(24):7130. https://doi.org/10.3390/s20247130

Choi GH, Lim K, Pan SB (2021) Driver identification system using normalized electrocardiogram based on adaptive threshold filter for intelligent vehicles. Sensors 21(1):202. https://doi.org/10.3390/s21010202

Choi GH, Lim K, Pan SB (2022a) Driver identification system using 2D ECG and EMG based on multi-stream CNN for Intelligent vehicle. IEEE Sens Lett 6(6):1–4. https://doi.org/10.1109/LSENS.2022.3175787

Choi GH, Lim K, Pan SB (2022b) Identification system based on resolution adjusted 2D spectrogram of driver's ECG for ıntelligent vehicle. Mobile Inf Syst. https://doi.org/10.1155/2022/5404343

Chong LS, Rabkin AN, Emhoff SM, Barry-Menkhaus S, Rivers AJ, Lehrbach M, Gordis EB (2022) Childhood harsh parenting and later aggression: non-violent discipline and resting skin conductance as moderators. J Aggress Maltreat Trauma 32(3):1–18

Cosme G, Tavares V, Nobre G, Lima C, Sá R, Rosa P, Prata D (2022) Cultural differences in vocal emotion recognition: a behavioural and skin conductance study in Portugal and Guinea-Bissau. Psychol Res 86:597–616

Dantcheva PE, Ross A (2015) What else does your biometric data reveal? A survey on soft biometrics. IEEE Trans Inf Forensics Secur 11(3):441–467

Dehzangi O, Rajendra V, Taherisadr M (2018) Wearable driver distraction identification on-the-road via continuous decomposition of galvanic skin responses. Sensors 18(2):503

El Mekki A, Bouhoute A, Berrada I (2019) Improving driver identification for the next-generation of in-vehicle software systems. IEEE Trans Veh Technol 68(8):7406–7415. https://doi.org/10.1109/TVT.2019.2924906

Fanti KA, Mavrommatis I, Georgiou G, Kyranides MN, Andershed H, Colins OF (2022) Extending the construct of psychopathy to

childhood: testing associations with heart rate, skin conductance, and startle reactivity. J Psychopathol Behav Assess 44:26–38
Farzin H, Abrishami-Moghaddam H, Moin MS (2008) A novel retinal identification system. EURASIP J Adv Signal Process 2008:280635
Ferrari C, Vecchi T, Sciamanna G, Blandini F, Pisani A, Natoli S (2021) Facemasks and face recognition: potential impact on synaptic plasticity. Neurobiol of Dis 153:105319
Fisher RA (1936) The use of multiple measurements in taxonomic problems. Ann Eugenic 7:179–188
Fung NC, Wallace B, Chan AD, Goubran R, Porter MM, Marshall S, Knoefel F (2017) Driver identification using vehicle acceleration and deceleration events from naturalistic driving of older drivers. In: 2017 IEEE ınternational symposium on medical measurements and applications (MeMeA). IEEE, pp 33–38. https://doi.org/10.1109/MeMeA.2017.7985845
Gjoreski M, Mahesh B, Kolenik T, Uwe-Garbas J, Seuss D, Gjoreski H, Luštrek M, Gams M, Pejović V (2021) Cognitive load monitoring with wearables–lessons learned from a machine learning challenge. IEEE Access 9:103325–103336
Goldberger AL, Amaral LAN, Glass L, Hausdorff JM, Ivanov PC, Mark RG, Mietus JE, Moody GB, Peng CK, Stanley HE (2000) PhysioBank, PhysioToolkit, and PhysioNet: components of a new research resource for complex physiologic signals. Circulation 101(23):e215–e220
Goshvarpour A, Goshvarpour A (2020) The potential of photoplethysmogram and galvanic skin response in emotion recognition using nonlinear features. Phys Eng Sci Med 43(1):119–134
Gowda HDS, Kumar GH, Imran M (2018) Multimodal biometric recognition system based on nonparametric classifiers. In: Lecture notes in networks and systems (43), data analytics and learning. Springer, pp 269–278
Han J, Lang A, Amon MJ (2022) Can media synchronize our physiological responses? Skin conductance synchrony as a function of message valence, arousal, and emotional change rate. Commun Monogr 89(1):47–69
He J, Chen J, Liu J, Li H (2019) A lightweight architecture for driver status monitoring via convolutional neural networks. In: 2019 IEEE ınternational conference on robotics and biomimetics (ROBIO). IEEE, pp 388–394
Healey JA, Picard RW (2005) Detecting stress during real-world driving tasks using physiological sensors. IEEE Trans Intell Transp Syst 6(2):156–166
Hwang HB, Kwon H, Chung B, Lee J, Kim IY (2021) ECG authentication based on non-linear normalization under various physiological conditions. Sensors 21(21):6966. https://doi.org/10.3390/s21216966
Iqbal T, Redon-Lurbe P, Simpkin AJ, Elahi A, Ganly S, Wijns W, Shahzad A (2021) A sensitivity analysis of biophysiological responses of stress for wearable sensors in connected health. IEEE Access 9:93567–93579
Işıklı Esener İ (2019) A novel stress-level-specific feature ensemble for drivers' stress level recognition. Bilecik Seyh Edebali Univ J Sci 6(1):12–23
Işıklı Esener İ (2021) Subspace-based feature extraction on multi-physiological measurements of automobile drivers for distress recognition. Biomed Signal Process Control 66:102504
Jafarnejad S, Castignani G, Engel T (2017) Towards a real-time driver identification mechanism based on driving sensing data. In: 2017 IEEE 20th ınternational conference on ıntelligent transportation systems (ITSC). IEEE pp 1–7. https://doi.org/10.1109/ITSC.2017.8317716
Jiang X, Xu K, Liu X, Dai C, Clifton DA, Clancy EA, Akay M, Chen W (2020) Neuromuscular password-based user authentication. IEEE Trans Industr Inf 17(4):2641–2652. https://doi.org/10.1109/TII.2020.3001612
Jin X, Tang J, Kong X, Peng Y, Cao J, Zhao Q, Kong W (2021) CTNN: A convolutional tensor-train neural network for multi-task brainprint recognition. IEEE Trans Neural Syst Rehabil Eng 29:103–112
Kanhangad V, Kumar A, Zhang D (2011) Contactless and pose ınvariant biometric ıdentification using hand surface. IEEE Trans Image Process 20(5):1415–1424
Keshan N, Parimi PV, Bichindaritz I (2015) Machine learning for stress detection from ECG signals in automobile drivers. In: 2015 IEEE conference on big data. IEEE, pp 2661–2669
Khan MU, Choudry ZA, Aziz S, Naqvi SZH, Aymin A, Imtiaz MA (2020e). Biometric authentication based on EMG signals of speech. In: 2020 ınternational conference on electrical, communication, and computer engineering (ICECCE). IEEE, pp 1–5. https://doi.org/10.1109/ICECCE49384.2020.9179354
Kim JS, Pan SB (2017) A study on EMG-based biometrics. J Internet Serv Inf Secur 7:19–31
Kim KM, Choi JI (2019) Passengers' gesture recognition model in self-driving vehicles: gesture recognition model of the passengers' obstruction of the vision of the driver. In: 2019 IEEE 4th ınternational conference on computer and communication systems (ICCCS). IEEE, pp 239–242
Kim JS, Kim SH, Pan SB (2020a) Personal recognition using convolutional neural network with ECG coupling image. J Ambient Intell Humaniz Comput 11(5):1923–1932
Kim MG, Ko H, Pan SB (2020b) A study on user recognition using 2D ECG based on ensemble of deep convolutional neural networks. J Ambient Intell Humaniz Comput 11(5):1859–1867
Kim J, Park J, Park J (2020c) Development of a statistical model to classify driving stress levels using galvanic skin responses. Hum Factors Man 30:321–328. https://doi.org/10.1002/hfm.20843
Kwak BI, Han ML, Kim HK (2020) Driver identification based on wavelet transform using driving patterns. IEEE Trans Ind Inf 17(4):2400–2410. https://doi.org/10.1109/TII.2020.2999911
Labati RD, Muñoz E, Piuri V, Sassi R, Scotti F (2019) Deep-ECG: convolutional neural networks for ECG biometric recognition. Pattern Recognit Lett 126:78–85
Lee M, Ryu, J, Youn I (2017) Biometric personal identification based on gait analysis using surface EMG signals. In: 2017 2nd IEEE ınternational conference on computational ıntelligence and applications (ICCIA). IEEE, pp 318–321. https://doi.org/10.1109/CIAPP.2017.8167230
Lei X, Zhang Y, Lu Z (2016) Deep learning feature representation for electrocardiogram identification. In: 2016 IEEE ınternational conference on digital signal processing (DSP). IEEE, pp 11–14
Li Q, Dong P, Zheng J (2020) Enhancing the security of pattern unlock with surface EMG-based. Biom Appl Sci 10(2):541. https://doi.org/10.3390/app10020541
Liew WS, Seera M, Loo CK, Lim E, Kubota N (2016) Classifying stress from heart rate variability using salivary biomarkers as reference. IEEE Trans Neural Netw Learn Syst 27(10):2035–2046
Lin SL, Chen CK, Lin CL, Yang WC, Chiang CT (2014) Individual identification based on chaotic electrocardiogram signals during muscular exercise. IET Biometrics 3(4):257–266
Liu J, Chen Y, Dong Y, Wang Y, Zhao T, Yao YD (2020) Continuous user verification via respiratory biometrics. In: IEEE INFOCOM 2020-IEEE conference on computer communications. IEEE, pp 1–10
Lu L, Mao J, Wang W, Ding G, Zhang Z (2019). An EMG-based personal identification method using continuous wavelet transform and convolutional neural networks. In: 2019 IEEE biomedical circuits and systems conference (BioCAS). IEEE pp 1–4. https://doi.org/10.1109/BIOCAS.2019.8919230

Lu L, Mao J, Wang W, Ding G, Zhang Z (2020) A study of personal recognition method based on EMG signal. IEEE Trans Biomed Circuits Syst 14(4):681–691

Lyamin AV, Cherepovskaya EN (2017) An approach to biometric ıdentification by using low-frequency eye tracker. IEEE Trans Inf Forensics Secur 12(4):881–891

Makowski D, Pham T, Lau Z, Brammer J, Lespinasse F, Pham H, Scholzel C, Chen S (2021) NeuroKit2: a python toolbox for neurophysiological signal processing. Behav Res Methods 53:1689–1696

Marchegiani L, Posner I (2018) Long-term driving behaviour modelling for driver identification. In: 2018 21st ınternational conference on ıntelligent transportation systems (ITSC). IEEE, pp 913–919. https://doi.org/10.1109/ITSC.2018.8569610

Martínez JP, Almeida R, Olmos S, Rocha AP, Laguna P (2004) A wavelet-based ECG delineator: evaluation on standard databases. IEEE Trans Biomed Eng 51(4):570–581

McLachlan GJ (1992) Logistic discrimination. In: McLachlan GJ (ed) Discriminant analysis and statistical pattern recognition. Wiley Online Library, pp 255–282

Miyaji M, Kawanaka H, Oguri K (2010a) Effect of pattern recognition features on detection for driver's cognitive distraction. In: 13th ınternational IEEE conference on ıntelligent transportation systems. IEEE, pp 605–610

Miyaji M, Kawanaka H, Oguri K (2010b) Study on effect of adding pupil diameter as recognition features for driver's cognitive distraction detection. In: 2010b 7th ınternational symposium on communication systems, networks & digital signal processing (CSNDSP 2010b). IEEE, pp 406–411

Miyajima C, Nishiwaki Y, Ozawa K, Wakita T, Itou K, Takeda K, Itakura F (2007) Driver modeling based on driving behavior and its evaluation in driver identification. Proc IEEE 95(2):427–437. https://doi.org/10.1109/JPROC.2006.888405

Momeni N, Valdés AA, Rodrigues J, Sandi C, Atienza D (2022) CAFS: cost-aware features selection method for multimodal stress monitoring on wearable devices. IEEE Trans Biomed Eng 69(3):1072–1084

Morikawa S, Ito SI, Ito M, Fukumi M (2018). Personal authentication by lips EMG using dry electrode and CNN. In: 2018 IEEE ınternational conference on ınternet of things and ıntelligence system (IOTAIS). IEEE, pp 180–183. https://doi.org/10.1109/IOTAIS.2018.8600859

Munla N, Khalil M, Shahin A, Mourad A (2015) Driver stress level detection using HRV analysis. In: 2015 international conference on advances in biomedical engineering (ICABME). IEEE, pp 61–64

Nath RK, Thapliyal H (2021) Smart wristband-based stress detection framework for older adults with cortisol as stress biomarker. IEEE Trans Consum Electron 67(1):30–39

Nazmy TM, El-Messiry H, Al-Bokhity B (2010). Adaptive neuro-fuzzy inference system for classification of ECG signals. In: 2010 the 7th international conference on informatics and systems (INFOS). IEEE, pp 1–6

Nishiwaki Y, Ozawa K, Wakita T, Miyajima C, Itou K, Takeda K (2007) Driver ıdentification based on spectral analysis of driving behavioral signals. In: Abut H, Hansen JHL, Takeda K (eds) Advances for ın-vehicle and mobile systems. Springer, Boston. https://doi.org/10.1007/978-0-387-45976-9_3

Nobunaga T, Tanaka H, Tanahashi I, Watanabe T, Hattori Y (2017) Optimised band-pass filter to ensure accurate ECG-based identification of exercising human subjects. Electron Lett 53(4):222–224

Norland K, Sveinbjornsson G, Thorolfsdottir RB, Olafur B, Davidsson B, Tragante V, Rajamani S, Helgadottir A, Gretarsdottir S, van Setten J, Asselbergs FW, Sverrisson JTh, Stephensen SS, Oskarsson G, Sigurdsson EL, Andersen K, Danielsen R, Thorgeirsson G, Thorsteinsdottir U, Arnar DO, Sulem P, Holm H, Gudbjartsson DF, Stefansson K (2019) Sequence variants with large effects on cardiac electrophysiology and disease. Nat Commun 10:4803

Nourbakhsh N, Chen F, Wang Y, Calvo RA (2017) Detecting users' cognitive load by galvanic skin response with affective interference. ACM Trans Interact Intelligent Systems (TiiS) 7(3):1–20

Pan J, Tompkins WJ (1985) A real-time QRS detection algorithm. IEEE Trans Biomed Eng BEM 32(3):230–236

Park K, Song M, Kim SY (2018) The design of a single-bit CMOS image sensor for iris recognition applications. Sensors (basel) 18(2):669

Pereira TMC, Conceição RC, Sebastião R (2022) Initial study using electrocardiogram for authentication and ıdentification. Sensors (basel) 22(6):2202

Pineau G, Jean E, Romo L, Villemain F, Poupon D, Gorwood P (2022) Skin conductance while facing emotional pictures at day 7 helps predicting antidepressant response at three months in patients with a major depressive episode. Psychiatry Res 309:114401

Pinto JR, Cardoso JS, Lourenço A, Carreiras C (2017) Towards a continuous biometric system based on ECG signals acquired on the steering wheel. Sensors 17(10):2228

Plev M, Korečko Š, Hladek D, Bours P, Skudal MH, Liao YF (2022) Biometric user ıdentification by forearm EMG analysis. In: 2022 IEEE ınternational conference on consumer electronics-Taiwan. IEEE, pp 607–608. https://doi.org/10.1109/ICCE-Taiwan55306.2022.9869268

Pradhan A, He J, Jiang N (2021) Performance optimization of surface electromyography based biometric sensing system for both verification and ıdentification. IEEE Sens J 21(19):21718–21729

Prakash S, Gupta P (2014) Human recognition using 3D ear ımages. Neurocomputing 140:317–325

Qin H, He X, Yao X, Li H (2017) Finger-vein verification based on the curvature in Radon space. Expert Syst Appl 82:151–161

Rahim MA, Zhu L, Li X, Liu J, Zhang Z, Qin Z, Khan S, Gai K (2020) Zero-to-stable driver identification: a non-intrusive and scalable driver identification scheme. IEEE Trans Veh Technol 69(1):163–171. https://doi.org/10.1109/TVT.2019.2954529

Ramalho MB, Correia PL, Soares LD (2012) Hand-based multimodal ıdentification system with secure biometric template storage. IET Comput vis 6(3):165–173

Rani BMS, Rani AJ (2019) A hybrid biometric identification and authentication system with retinal verification using AWN classifier for enhancing security. In: Advances in intelligent systems and computing, first international conference on artificial intelligence and cognitive computing. Springer, Singapore, pp 561–569

Rezgui D, Lachiri Z (2016) ECG biometric recognition using SVM-based approach. IEEJ Trans Electr Electron Eng 11(S1):S94–S100

Safavian SR, Landgrebe D (1991) A survey of decision tree classifier methodology. IEEE Trans Syst Man Cybern 21:660–674

Santos A, Medeiros I, Resque P, Rosário D, Nogueira M, Santos A, Cerqueira EC, Chowdhury KR (2018) ECG-based user authentication and identification method on VANETs. In: Proceedings of the 10th Latin America networking conference, pp 119–122

Seha SNA, Hatzinakos D (2020) EEG-based human recognition using steady-state AEPs and subject-unique spatial filters. IEEE Trans Inf Forensics Secur 15:3901–3910

Setyohadi DB, Kusrohmaniah S, Gunawan SB, Pranowo P (2018) Galvanic skin response data classification for emotion detection. Int J Electr Comput Eng (IJECE) 8(5):31–41

Shin S, Jung J, Kim YT (2017) A study of an EMG-based authentication algorithm using an artificial neural network. In:

2017 IEEE SENSORS. IEEE, pp 1–3. https://doi.org/10.1109/ICSENS.2017.8234158
Shioji R, Ito SI, Ito M, Fukumi M (2017) Personal authentication based on wrist EMG analysis by a convolutional neural network. In: Proceedings of the 5th IIAE ınternational conference on ıntelligent systems and ımage processing, pp 12–18
Shioji R, Ito SI, Ito M, Fukumi M (2018) Personal authentication and hand motion recognition based on wrist EMG analysis by a convolutional neural network. In: 2018 IEEE ınternational conference on ınternet of things and ıntelligence system (IOTAIS). IEEE, pp 184–188. https://doi.org/10.1109/SCIS-ISIS.2018.00184
Shiwu L, Linhong W, Zhifa Y, Bingkui J, Feiyan Q, Zhongkai Y (2011) An active driver fatigue identification technique using multiple physiological features. In: 2011 ınternational conference on mechatronic science, electric engineering and computer (MEC). IEEE, pp 733–737
Sihem NITA, Bitam S, Mellouk A (2019) A body area network for ubiquitous driver stress monitoring based on ECG signal. In: 2019 ınternational conference on wireless and mobile computing, networking and communications (WiMob). IEEE, pp 1–6
Silva H, Lourenço A, Fred A (2012) In-vehicle driver recognition based on hand ECG signals. In: Proceedings of the 2012 ACM international conference on ıntelligent user ınterfaces, pp 25–28
Singh RK, Sarkar A, Anoop CS (2016) A health monitoring system using multiple non-contact ECG sensors for automotive drivers. In: 2016 IEEE ınternational ınstrumentation and measurement technology conference proceedings. IEEE, pp 1–6
Song T, Cheng X, Li H, Yu J, Wang S, Bie R (2016) Detecting driver phone calls in a moving vehicle based on voice features. In: IEEE INFOCOM 2016-the 35th annual IEEE ınternational conference on computer communications. IEEE, pp 1–9
Spelt HAA, Westerink JHDM, Ham J, Ijsselsteijn WA (2022) Psychophysiological reactions to persuasive messages deploying persuasion principles. IEEE Trans Affect Comput 13(1):461–472
Srivastva R, Singh A, Singh YN (2021) Plexnet: a fast and robust ECG biometric system for human recognition. Inf Sci 558:208–228
Srivastva R, Singh YN, Singh A (2022) Statistical independence of ECG for biometric authentication. Pattern Recognit 127:108640
Tiwari S, Agarwal S (2021) A shrewd artificial neural network-based hybrid model for pervasive stress detection of students using galvanic skin response and electrocardiogram signals. Big Data 9(6):427–442
Wang Y, Xie W, Yu X, Shark LK (2015) An automatic physical access control system based on hand vern biometric ıdentification. IEEE Trans Consum Electron 61(3):320–327
Wang L, Li J, Wang Y (2019) Modeling and recognition of driving fatigue state based on RR intervals of ECG data. IEEE Access 7:175584–175593
Wang M, Hu J, Abbass HA (2020a) BrainPrint: EEG biometric identification based on analyzing brain connectivity graphs. Pattern Recognit 105:107381
Wang X, Guo Y, Ban J, Xu Q, Bai C, Liu S (2020b) Driver emotion recognition of multiple-ECG feature fusion based on bp network and d–s evidence. IET Intell Transp Syst 14:815–824
Wang X, Li F, Xie Y, Yang S, Wang Y (2022a) Gait and respiration-based user identification using Wi-Fi signal. IEEE Internet Things J 9(5):3509–3521
Wang Y, Gu T, Luan TH, Yu Y (2022b) Your breath doesn't lie: multi-user authentication by sensing respiration using mmWave radar. In: 2022b 19th annual IEEE ınternational conference on sensing, communication, and networking (SECON). IEEE, pp 64–72
Wang D, Wang C, Yi X, Sai L, Fu G, Lin XA (2022c) Detecting concealed information using functional near-infrared spectroscopy (fNIRS) combined with skin conductance, heart rate, and behavioral measures. Psychophysiology 59(8):e14029
Webb AR (2002) Linear discriminant analysis. In: Webb AR (ed) Statistical pattern recognition. Wiley Online Library, pp 123–124
Wieclaw L, Khoma Y, Fałat P, Sabodashko D, Herasymenko V (2017) Biometrie identification from raw ECG signal using deep learning techniques. In: 2017 9th IEEE ınternational conference on ıntelligent data acquisition and advanced computing systems: technology and applications (IDAACS), vol 1. IEEE, pp 129–133
Wilaiprasitporn T, Ditthapron A, Matchaparn K, Tongbuasirilai T, Banluesombatkul N, Chuangsuwanich E (2019) Affective EEG-based person identification using the deep learning approach. IEEE Trans Cogn Develop Syst 12(3):486–496
Wiltshire CN, Wanna CP, Stenson AF, Minton ST, Reda MH, Davie WM, Hinrichs R, Winters S, France JM, Jovanovic T (2022) Associations between children's trauma-related sequelae and skin conductance captured through mobile technology. Behav Res Ther 150:104036
Wu JD, Ye SH (2009) Driver identification using finger-vein patterns with Radon transform and neural network. Expert Syst Appl 36(3):5793–5799. https://doi.org/10.1016/j.eswa.2008.07.042
Yang J, Zhang D, Yang J-y, Niu B (2007) Globally maximizing, locally minimizing: unsupervised discriminant projection with applications to face and palm biometrics. IEEE Trans Pattern Anal Mach Intell 29(4):650–664
Zangeneh E, Rahmati M, Mohsenzadeh Y (2020) Low resolution face recognition using a two-branch deep convolutional neural network architecture. Expert Syst Appl 139:112854
Zeng F, Hu S, Xiao K (2019) Research on partial fingerprint recognition algorithm based on deep learning. Neural Comput Appl 31(9):4789–4798
Zhang W, Cheng B, Lin Y (2012) Driver drowsiness recognition based on computer vision technology. Tsinghua Sci Technol 17(3):354–362
Zhang X, Yao L, Huang C, Gu T, Yang Z, Liu Y (2020) DeepKey: a multimodal biometric authentication system via deep decoding gaits and brainwaves. ACM Trans Intell Syst Technol 11(4):49
Zhang M, Liu R, Deguchi D, Murase H (2022) Masked face recognition with mask transfer and self-attention under the COVID-19 pandemic. IEEE Access 10:20527–20538
Zhao D, Hou J, Zhong Y, He W, Fu Z, Zhou F (2022) Driver identification methods in electric vehicles, a review. World Electr Vehicle J 13(11):207. https://doi.org/10.3390/wevj13110207
Zhou R, Wang C, Zhang P, Chen X, Du L, Wang P, Zhao Z, Du M, Fang Z (2021) ECG-based biometric under different psychological stress states. Comput Methods Programs Biomed. https://doi.org/10.1016/j.cmpb.2021.106005